Parametric Study on Arc Behavior of Magnetically Diffused Arc

2016 Plasma Sci. Technol. 18 6

(http://iopscience.iop.org/1009-0630/18/1/6)

Parametric Study on Arc Behavior of Magnetically Diffused Arc*

CHEN Tang (陈塘)[1], LI Hui (李辉)[1], BAI Bing (白冰)[1,2], LIAO Mengran (廖梦然)[1], XIA Weidong (夏维东)[1]

[1]Department of Thermal Science and Energy Engineering, University of Science and Technology of China, Hefei 230027, China
[2]Full Dimension Power Tech. Co., Ltd, Beijing 100085, China

Abstract A model coupling the plasma with a cathode body is applied in the simulation of the diffuse state of a magnetically rotating arc. Four parametric studies are performed: on the external axial magnetic field (AMF), on the cathode shape, on the total current and on the inlet gas velocity. The numerical results show that: the cathode attachment focuses in the center of the cathode tip with zero AMF and gradually shifts off the axis with the increase of AMF; a larger cathode conical angle corresponds to a cathode arc attachment farther away off axis; the maximum values of plasma temperature increase with the total current; the plasma column in front of the cathode tip expands more severely in the axial direction, with a higher inlet speed; the cathode arc attachment shrinks towards the tip as the inlet speed increases. The various results are supposed to be explained by the joint effect of coupled cathode surface heating and plasma rotating flow.

Keywords: arc modeling, cathode arc attachment, plasma configuration

PACS: *52.25.Kn, 52.80.Mg*

DOI: 10.1088/1009-0630/18/1/02

(Some figures may appear in colour only in the online journal)

1 Introduction

A wide range of numerical simulations based on computational fluid dynamics coupled with electromagnetics have been carried out [1−4], to achieve basic understanding of the arc discharge. The cathode arc attachment plays a key role in the discharge process, and is highly related to the cathode body temperature since the thermal emission current dominates the major part of the current through the cathode surface [5]. Therefore, a modeling of arc discharge including the cathode body is able to predict the cathode temperature and the cathode arc attachment state.

Non-transferred dc plasma torches have been widely used for material processing/preparation, environmental protection and chemical production, since the plasma jet generated is able to accelerate and melt the injected powdered materials [6,7]. One typical case is a plasma torch with arc discharge between a rod-type cathode and a hollow anode. The erosion of electrode materials due to high current density and heat flux within arc attachments, can be reduced by the external axial magnetic field. The external magnetic field forces not only the arc plasma but also the attachment to rotate [8,9]. Magnetically rotating arcs have been increasingly adopted in dc arc plasma devices for diagnostics and material processing, modern circuit breakers, etc [8,10]. Though previous studies [10−12] are sufficient enough to reveal the structure of the rotating arc column, in 2D assumption [12−15] or 3D assumption [10,16], they do not focus on the variation of cathode temperature and cathode arc attachment behavior under different simulation conditions.

Therefore, a self-consistent local thermodynamic equilibrium (LTE) model for DC arc plasmas is described, in order to unify the thermionic cathode and the arc column. In the region near the cathode, the ambipolar diffusion assumption of ion-electron is adopted. The modeling neglects the space charge layer in front of the cathode surface. At the same time the electrical conductivity is modified according to the number density of electrons. This model has been widely used in many previous studies concerning free burning argon arc [17−21] and the calculation results appear to be consistent with the experiments. The cathode arc attachment is assumed to be variable. This should bring along influences on the flow and thermal conduction state of the arc column [22]. The aim of this paper is to carry out the simulation on the effect of several physical parameters, as inlet gas velocity, external axial magnetic field, cathode shape and total current.

2 Numerical model

2.1 Arc column model

In this study of high intensity argon arc at atmospheric pressure with an arc current of about 100-300 A, the LTE state is a reasonable approximation for the arc column region [23]. Experimental results show

*supported by National Natural Science Foundation of China (Nos. 11475174, 11035005 and 50876101)

that the behavior of rotating plasma under AMF is 3 dimensional and time-dependent [8]. However, the axisymmetric and steady state assumptions are adopted in this paper for such reasons: (1) modeling in this paper can be seen as a simplified first step to a more realistic and complex one; (2) the magnetically rotating arc exists in two modes: contracted and diffused, in the latter mode, in quite a large area, the plasma is observed to be homogeneous [8]; (3) the diffuse state can be maintained once the experimental condition is proper [8] and the simulation is not focused on the evolution process of arc discharge. Therefore, simulation in this paper can be taken as a time-average estimation of magnetically rotating arc in diffuse mode.

Thus the simulation is based on the following assumptions: (a) the plasma flow is swirling, axisymmetric, steady, and turbulent; (b) plasma is in the LTE state and optically thin to radiation; (c) the motional electric field is neglected, but Lorentz force generated by the self-induced magnetic field is taken into account; (d) the influence of the pressure gradient work and gravity effect is neglected. According to the assumptions, the governing equations in cylindrical coordinates (z, r) are as follows.

Mass conservation equation:

$$\frac{1}{r}\frac{\partial}{\partial r}(r\rho v_r)+\frac{\partial}{\partial z}(\rho v_z)=0. \tag{1}$$

Momentum conservation equations:

$$\frac{1}{r}\frac{\partial}{\partial r}(r\rho v_r^2)+\frac{\partial}{\partial z}(\rho v_r v_z)=-\frac{\partial P}{\partial r}+\frac{1}{r}\frac{\partial}{\partial r}(2r\Gamma_{\mathrm{u}}\frac{\partial v_r}{\partial r}) +\frac{\partial}{\partial z}(\Gamma_{\mathrm{u}}\frac{\partial v_r}{\partial z}+\Gamma_{\mathrm{u}}\frac{\partial v_z}{\partial r})-2\Gamma_{\mathrm{u}}\frac{v_r}{r^2}+F_r. \tag{2}$$

$$\frac{1}{r}\frac{\partial}{\partial r}(r\rho v_r v_z)+\frac{\partial}{\partial z}(\rho v_z^2)=-\frac{\partial P}{\partial z}+\frac{\partial}{\partial r}(2\Gamma_{\mathrm{u}}\frac{\partial v_z}{\partial z}) +\frac{1}{r}\frac{\partial}{\partial r}(r\Gamma_{\mathrm{u}}\frac{\partial v_r}{\partial z}+\Gamma_{\mathrm{u}}\frac{\partial v_z}{\partial r})+F_z. \tag{3}$$

$$\frac{1}{r}\frac{\partial}{\partial r}(r\rho v_r v_\theta)+\frac{\partial}{\partial z}(\rho v_z v_\theta)=\frac{\partial}{\partial z}(\Gamma_{\mathrm{u}}\frac{\partial v_\theta}{\partial z}) +\frac{1}{r}\frac{\partial}{\partial r}\Gamma_{\mathrm{u}}(r\frac{\partial v_\theta}{\partial r}-v_\theta)+\frac{2}{r}\Gamma_{\mathrm{u}}(\frac{\partial v_\theta}{\partial r}-\frac{v_\theta}{r})-\rho\frac{v_r v_\theta}{r}+F_\theta. \tag{4}$$

Energy conservation equation:

$$\frac{1}{r}\frac{\partial}{\partial r}(r\rho v_r h)+\frac{\partial}{\partial z}(\rho v_z h)=\frac{1}{r}\frac{\partial}{\partial r}(r\Gamma_T\frac{\partial T}{\partial r})+\frac{\partial}{\partial z}(\Gamma_T\frac{\partial T}{\partial z}) +\frac{j_z^2+j_r^2}{\sigma}+U+\frac{5}{2}\frac{k}{e}(\frac{j_z}{C_{\mathrm{p}}}\frac{\partial h}{\partial z}+\frac{j_r}{C_{\mathrm{p}}}\frac{\partial h}{\partial r}). \tag{5}$$

Electric potential equation:

$$\frac{1}{r}\frac{\partial}{\partial r}(r\sigma\frac{\partial \varphi}{\partial r})+\frac{\partial}{\partial z}(\sigma\frac{\partial \varphi}{\partial r})=0. \tag{6}$$

Magnetic potential equations:

$$\frac{1}{r}\frac{\partial}{\partial r}(r\sigma\frac{\partial A_z}{\partial r})+\frac{\partial}{\partial z}(\sigma\frac{\partial A_z}{\partial z})=-\mu_0 j_z, \tag{7}$$

$$\frac{1}{r}\frac{\partial}{\partial r}(r\sigma\frac{\partial A_r}{\partial r})+\frac{\partial}{\partial z}(\sigma\frac{\partial A_r}{\partial z})=-\mu_0 j_r+\frac{A_r}{r^2}, \tag{8}$$

$$B_\theta=\frac{\partial A_r}{\partial r}-\frac{\partial A_z}{\partial r}. \tag{9}$$

Here v_r, v_z and v_θ are the radial, axial and tangential component of mass average velocity $\mathbf{v}$, ρ, p, T, and h are the plasma density, pressure, temperature of arc, and enthalpy respectively. μ, κ, σ, and U are the temperature-dependent plasma properties (in laminar flow state) of viscosity, thermal conductivity, electric conductivity, and radiation power per unit volume respectively. Γ_{u} and Γ_{T} are plasma viscosity and thermal conductivity in a turbulent state. j_r and j_z are radial and axial current density $\mathbf{j}=\sigma\mathbf{E}$. B_θ and B_z are the self-induced and external axial components of magnetic field $\mathbf{B}$. F_θ, F_r and F_z are tangential, radial and axial component of body forces $\mathbf{F}=\mathbf{j}\times\mathbf{B}$.

Previous studies indicate that, a back flow region emerges in front of the cathode surface. The intensive vortexes lead to a stronger mixture of cold and hot gas. An extra cooling effect intensified by turbulence may happen in this back flow region. For this reason, the turbulent equations are introduced in the plasma fluid region.

RNG (Re-normalization group) K-ϵ turbulent equations:

$$\frac{1}{r}\frac{\partial}{\partial r}(r\rho v_r K)+\frac{\partial}{\partial z}(\rho v_z K)=\frac{1}{r}\frac{\partial}{\partial}(r\alpha_{\mathrm{t}}\mu_{\mathrm{t}}\frac{\partial K}{\partial r}) +\frac{\partial}{\partial z}(\alpha_{\mathrm{t}}\mu_{\mathrm{t}}\frac{\partial K}{\partial z})+G-\rho\epsilon, \tag{10}$$

$$\frac{1}{r}\frac{\partial}{\partial r}(r\rho v_r \epsilon)+\frac{\partial}{\partial z}(\rho v_z \epsilon)=\frac{1}{r}\frac{\partial}{\partial_r}(r\alpha_\epsilon\mu_{\mathrm{t}}\frac{\partial \epsilon}{\partial r}) +\frac{\partial}{\partial z}(\alpha_\epsilon\mu_{\mathrm{t}}\frac{\partial \epsilon}{\partial z})+\frac{\epsilon}{k}(c_1 G-c_2\rho\epsilon)-R_\epsilon, \tag{11}$$

$$G=\mu_{\mathrm{t}}2\Big\{\Big[(\frac{\partial v_z}{\partial z})^2+(\frac{\partial v_r}{\partial r})^2+(\frac{v_r}{r})^2\Big]+(\frac{\partial v_z}{\partial r}+\frac{\partial v_r}{\partial z})^2 +(\frac{\partial v_\theta}{\partial z})^2+(\frac{\partial v_\theta}{\partial r}-\frac{v_\theta}{r})^2\Big\}, \tag{12}$$

$$R_\epsilon=\frac{c_\mu\rho\eta^3(1-\eta/\eta_0)}{1+\beta\eta^3}\frac{\epsilon^2}{K},$$

$$\Gamma_{\mathrm{u}}=\mu+\mu_{\mathrm{t}},\ \ \Gamma_T=\kappa+\frac{\mu_{\mathrm{t}}c_{\mathrm{p}}}{Pr_{\mathrm{t}}},\ \ \eta=S\frac{K}{\epsilon}, \tag{13}$$

K, ϵ, S and $\mu_{\mathrm{t}}=\frac{\rho c_{\mathrm{p}}K^2}{\epsilon}$ are turbulent kinetic energy, turbulent dissipation rate, norm of turbulent strain rate, and turbulent viscosity. $Pr_{\mathrm{t}}=0.9$, c_μ=0.085, β=0.012, η_0=4.38, α_{t}=1.39, α_ϵ=1.39, c_1=1.42, and c_2=1.68 are the model constants suggested by Yakhot and Orszag [24,25].

In energy conservation equations, it is assumed that the viscous dissipation and the work of the pressure gradient can be neglected due to the low Mach number.

2.2 Cathode heating model

To unify the plasma column and the cathode, a model presented by J. J. Lowke [19] is used. This method neglects the space-charge layer. In the near-cathode region (about 0.1 mm thickness), electron number density continuity equation accounting for ambipolar diffusion is solved, and the electric conductivity is modified according to the electron number density as follows:

$$\sigma_{\text{eff}} = \frac{n_{\text{e}} e}{n_0/(n_{\text{T}}\mu_{\text{e}}) + (2en_{\text{e}}n_{\text{eq}})/(n_{\text{T}}\sigma)}, \tag{14}$$

where n_0 is the equilibrium neutral particle density, μ_{e} is the electron mobility, n_{eq} is the equilibrium electron density, n_{e} is the electron number density calculated using ambi-polar diffusion assumption, and $n_{\text{T}} = n_0 + 2n_{\text{e}}$ is the total particle density. The ambi-polar diffusion equation for electrons is as follows [19]:

$$\nabla \cdot (-D_{\text{A}} \nabla n_{\text{e}}) = \dot{n}_{\text{i}}, \tag{15}$$

here, the net ionization rate is $\dot{n}_{\text{i}} = \alpha_{\text{re}}(G n_{\text{e}} n_0 - n_{\text{e}}^3)$, and G is the Saha function: $G = n_{\text{eq}}^2/n_0$. The three-body recombination coefficient α_{re} is taken from [20]. The ambipolar diffusion coefficient D_{A} is calculated from the method of Ref. [26].

The energy flux from plasma to cathode surface is as follows:

$$F_{\text{ca}} = -\varepsilon\alpha T_{\text{c}}^4 - j_{\text{e}}\Phi_{\text{c}} + j_{\text{i}}V_{\text{i}} - k\frac{\text{d}T}{\text{d}n}, \tag{16}$$

$$j_{\text{R}} = AT_{\text{c}}^2 \exp\frac{-\Phi_{\text{c}} e}{k_{\text{B}} T_{\text{c}}}, \tag{17}$$

where, ε, T_{c}, α, Φ_{c}, and V_{i} are the emissivity of the surface, the cathode temperature, the Stefan-Boltzmann constant, the work function, and the ionization potential respectively. j_{e}, j_{R} are the electron current density and theoretical thermionic emission current density given by the Richardson equation. A is the thermionic emission constant for the surface of the cathode, e is the electronic charge, and k_{B} is Boltzmann's constant. j, the current density at the surface of the cathode, can be obtained from the current continuity equation. At the cathode surface, j_{i} and j_{e} are set to $j - j_{\text{R}}$ and j_{R} respectively, when j is larger than j_{R}. They will be set to 0 and j respectively, when j is smaller than j_{R}. For a cathode made of pure tungsten, the Richardson constant $A = 1.2 \times 10^6$ AK^{-2} m^{-2} [27], the work function Φ_{c}=4.55 V [28], and the thermal conductivity $k = (1.86 - 0.0737T_{\text{c}} + 1.36 \times 10^{-5}T_{\text{c}}^2)$ W/m.

2.3 Domain and boundary conditions

The calculation domain consists of a cathode, near-cathode region and arc column, as shown in Fig. 1. The calculation domain is around 35 mm in radius and 75 mm in length, much larger than the arc plasma area formed in front of the cathode tip, so that the influence of inlet and outlet on the accuracy of results can be reduced to the minimum. In the cathode body solid thermal conduction and electric potential equations are solved. The cathode is assumed to be made of pure tungsten.

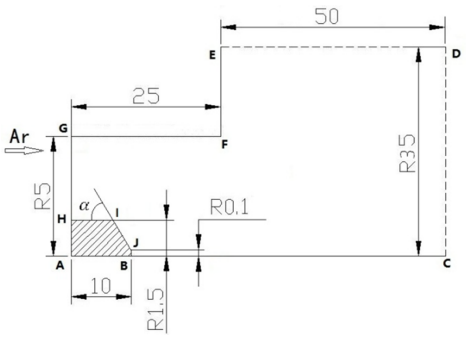

Fig.1 Scheme of half section of simulation domain

The boundary conditions of the primary variables are summarized in Table 1. A-B-C is the axis of symmetry of the system, where the axially symmetric conditions are employed for the independent variables. H-G is the gas inlet, H-I-J-B is the plasma-cathode interface, and E-D-C is the gas outlet. At the gas inlet, the boundary conditions for turbulent kinetic energy and its dissipation rate are taken as $K = 0.005u_{\text{in}}^2$ and $\epsilon = 0.1\rho K^2/\mu$, which are typically used in hydraulic flow calculations. At the gas outlet, $\dfrac{\partial K}{\partial n} = 0$ and $\dfrac{\partial \epsilon}{\partial n} = 0$. At A-H, the cathode bottom, current density is a given constant j_{in} and the temperature is set to 1000 K. Speculating from simulation and experimental results [19], if one set 300 K of temperature at A-H, too severe cooling may happen. If one uses a value of more than 2000 K, the cathode should be too hot. In a previous study [29] the cathode bottom temperature is set to 1500 K for an 8.4 mm cathode length (in this study cathode length equals 10 mm). Thus the temperature at A-H is set to the uniform value 1000 K. At anode surface G-F, the temperature is set to 1000 K, following papers [29–31].

Table 1. Boundary conditions

Boundary	T	P	ν	φ	A
H-G	300 K	1 atm	0.5-1.1 m/s	$\frac{\partial \varphi}{\partial n} = 0$	$\frac{\partial A}{\partial n} = 0$
E-D-C	Backflow T 300 K	$\frac{\partial P}{\partial n} = 0$	$\frac{\partial v}{\partial n} = 0$	$\frac{\partial \varphi}{\partial n} = 0$	$\frac{\partial A}{\partial n} = 0$
G-F	1000 K	-	-	$\varphi = 0$	$\frac{\partial A}{\partial n} = 0$
H-I-J-B	flux F_{ca}	-	0	coupled	coupled
A-H	1000 K	-	-	$j - j_{\text{in}}$	$\frac{\partial A}{\partial n} = 0$

3 Results and discussions

3.1 Comparison with "fixed" method

The cathode arc attachment distribution state can be seen from Fig. 2. In Fig. 2 temperature and current density profiles along the cathode conical surface are plotted, for four different external axial magnetic fields. The horizontal ordinate represents the distance to conical surface foot I, measured along the generatrix. Thus point I corresponds to distance 0 mm. The contour map of temperature is illustrated in Fig. 3 for I=200 A, B_z=0.15 T, inlet speed 0.5 m/s. For the purpose of comparison, we also give the results from modeling,

which fix temperature (3500 K) and total current density (1.1×10^8 A/m^2, restricted in $r \leq 5.426 \times 10^{-4}$ m) on the cathode surface. The cathode heating model in this paper allows the variation of arc attachment on the cathode surface and is labeled as "coupled". The method using fixed arc attachment is labeled as "fixed".

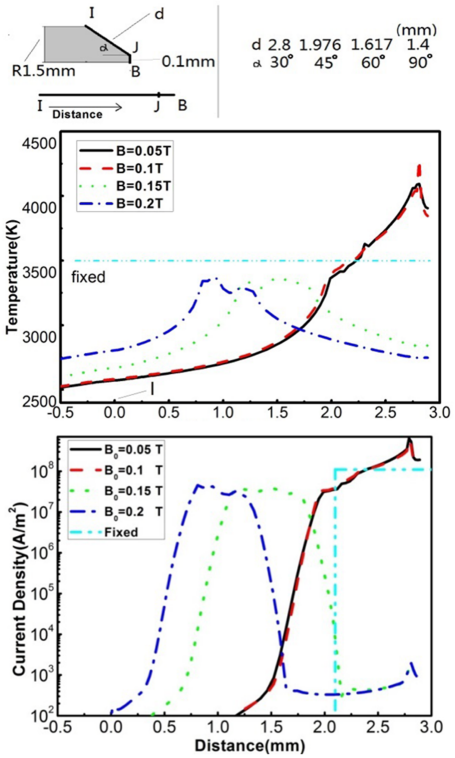

Fig.2 The temperature and current density distribution along the cathode surface, for four different external axial magnetic fields, I=200 A, inlet speed 0.5 m/s

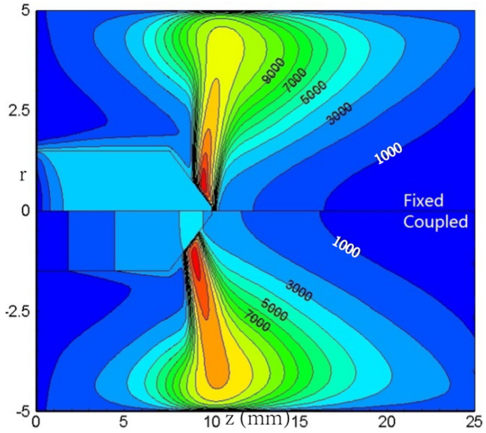

Fig.3 Maps of plasma temperature, I=200 A, B_z=0.15 T inlet speed 0.5 m/s

The maximum temperature of the arc column locates close to the cathode tip for the 'fixed' model and off axis near the middle of the cathode conical surface for the 'coupled' method (AMF 0.15 T). The maximum value of arc temperature is 16111 K and 13591 K for 'fixed' and 'coupled' models respectively. The maximum temperature of the "coupled" method (AMF 0.15 T) is lower and the sound explanation is that: the cathode arc attachment of "coupled" (AMF 0.15 T) is farther from the axis than "fixed"; its peak current density (Fig. 2, 0.015 T) is lower.

The contours of plasma temperature are illustrated in Fig. 4, for four different AMFs. For $B_z = 0.05$ T, 0.1 T, the cathode arc attachments are a spot shape. For B_z = 0.15 T, 0.2 T, the cathode arc attachments exhibit a ring shape. The maximum of temperature is around 2.2×10^4 K, 1.8×10^4 K, 1.3×10^4 K and 1.2×10^4 K and for B_z = 0.05 T, 0.1 T, 0.15 T and 0.2 T respectively. It is interesting to notice that, as the axial magnetic field increases, the arc attachment is farther and farther away off the axis. This phenomenon can be taken as a joint effect of plasma swirling and "coupled" cathode surface heating. On one hand, the Lorentz forces generated by AMF induce the tangential swirling of plasma. As a result the arc column should be dragged farther off axis with higher AMF (thus stronger centrifugal flow). On the other hand, the heating flux to cathode $F_{\mathrm{ca}} = -\varepsilon\alpha T_{\mathrm{c}}^4 - j_{\mathrm{e}}\Phi_{\mathrm{c}} + j_{\mathrm{i}}V_{\mathrm{i}} - k\dfrac{\mathrm{d}T}{\mathrm{d}n}$ increases with j_{i} and $-k\dfrac{\mathrm{d}T}{\mathrm{d}n}$. j_{i} and $-k\dfrac{\mathrm{d}T}{\mathrm{d}n}$ are decided by the column temperature in the near-cathode region. This indicates F_{ca} should evolve with the change of arc column shape and its peak value should move farther off axis as AMF increases. Therefore, the peak of the temperature of the cathode solid surface should move farther off axis with a higher AMF. The joint effect of plasma swirling and "coupled" cathode heating is already pointed out by the previous study of a free burning arc [22], in which the cathode attachment shrinks to the cathode tip as AMF increases.

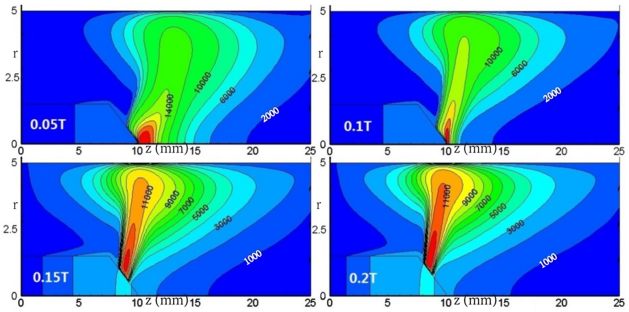

Fig.4 Maps of plasma temperature for four different external axial magnetic fields, $I = 200$ A, inlet speed 0.5 m/s

3.2 Parametric study

Contour maps of temperature for different half cone angles $\alpha = 30^{\mathrm{o}}$, $\alpha = 45^{\mathrm{o}}$, $\alpha = 60^{\mathrm{o}}$, $\alpha = 90^{\mathrm{o}}$ are plotted in Fig. 5. The corresponding temperature and current density distributions along the cathode surface are illustrated in Fig. 6. For a different cone angle, the plasma temperature distributions differ greatly from each other. The cathode arc attachment center locates in the front of the tip for $\alpha = 30^{\mathrm{o}}$, $\alpha = 45^{\mathrm{o}}$, in the middle of the conical surface for $\alpha = 60^{\mathrm{o}}$ and in the foot of the conical surface for $\alpha = 90^{\mathrm{o}}$. The temperature profile on the cathode conical surface is quite similar to the current density profile. The position of the maximum

cathode temperature corresponds to where the maximum current density locates. The maximum temperature is around 3800 K, 4200 K, 3500 K, and 3300 K for $\alpha = 30^o$, $\alpha = 45^o$, $\alpha = 60^o$, $\alpha = 90^o$ respectively. In a word, as the conical angle increases, the cathode arc attachment gradually moves off the axis towards the foot of the conical surface. A proper explanation is that, the arc column exists from a centrifugal flow caused by the tangential swirling. The centrifugal forces tend to drag the arc attachment towards the cathode conical surface foot I, as shown in Figs. 2 and 4. At the same time the plasma arc discharge without the consideration of swirling tends to force the arc attachment [19] shrinking to the cathode tip as a result of the plasma jet. The plasma jet flow is stronger with a smaller conical angle. The two effects have a balance point when the cathode arc spot moves to a certain place on the conical surface. As a result, under a certain AMF, the arc attachment locates nearer to the cathode tip with a smaller cathode conical angle.

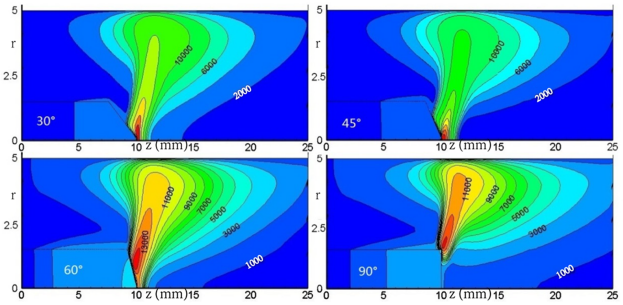

Fig.5 Maps of plasma temperature for different cathode shapes, inlet speed 0.5 m/s, B_z=0.1 T, α=30°, 45°, 60°, 90°

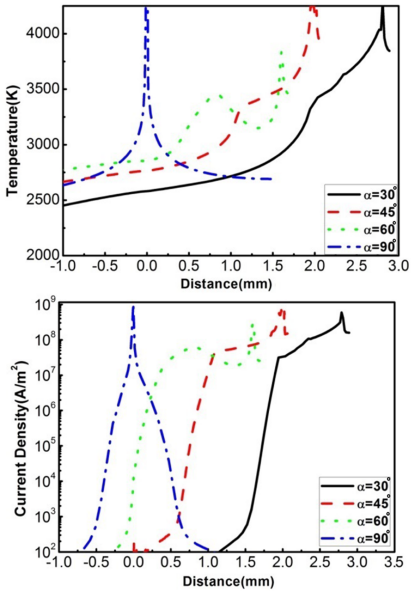

Fig.6 Profiles of temperature and current density along cathode conical surface, for different cathode shape, I=200 A, inlet speed 0.5 m/s, B_z=0.1 T, α=30°, 45°, 60°, 90°

The influences of the total current and inlet velocity speed on the plasma temperature distribution are illustrated in Figs. 7 and 8. As the total current increases, the shape of the plasma remains the same. At the same time, the volume of the high temperature region (T > 6000 K) expands. The maximum value of temperature equals 1.4×10^4 K, 1.8×10^4 K and 2.2×10^4 K for total current 100 A, 200 A and 300 A respectively. The increase of the peak temperature of the arc column is supposed to be related to the current density increase as Fig. 9 shows.

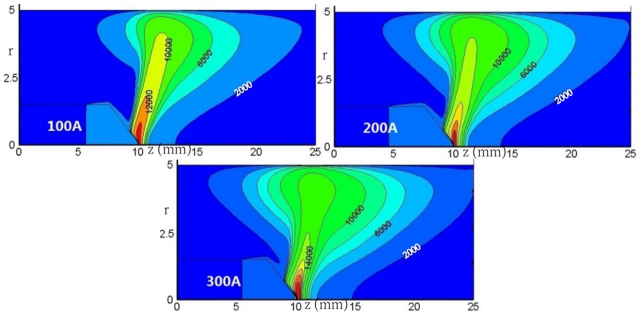

Fig.7 Maps of plasma temperature for different total current, inlet speed 0.5 m/s, B_z=0.1 T, α= 45°

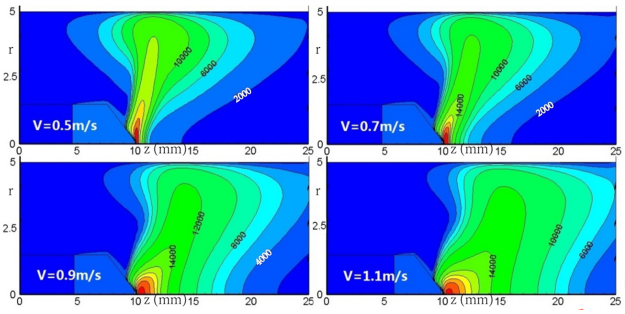

Fig.8 Maps of plasma temperature for different inlet speed V, B_z=0.1 T, I=200 A, α=45°

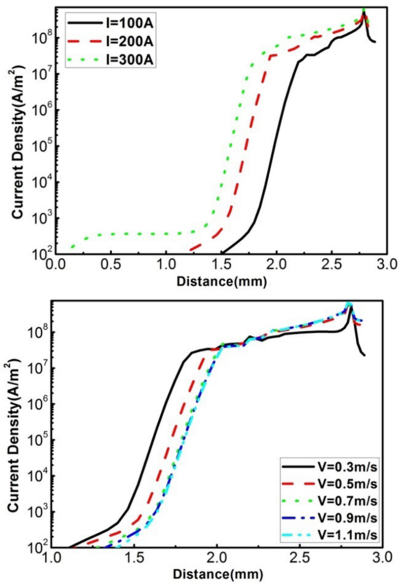

Fig.9 Profiles of current density along the cathode conical surface for different total current and different inlet velocity speed

It is interesting to notice from Fig. 8 that the inlet gas speed has a dramatic influence on the plasma configuration. The plasma near the anode moves towards the outlet as V increases. The whole arc column seems more oblique with a higher inlet velocity. Increasing

the inlet velocity, the plasma backflow speed decreases as a result of the momentum conservation. The backflow from the outer region of the torch has an effect to bring in cold gas and cool the arc column. Thus as V increases, the high temperature area ($T > 6000$ K) greatly expands towards the outlet as a result of a reduction of cooling from the outer region gas. Along with the increase of cooling from inlet gas, the whole plasma structure shifts towards the outlet.

The corresponding current density profiles of different total current and different inlet velocity are plotted in Fig. 9. The temperature profiles are not included since their configurations and variations are quite similar to the current density. As the total current increases, the cathode arc attachment expands and the maximum current density is enhanced. As Fig. 9 shows, with the increase of inlet velocity, the cathode arc attachment shrinks towards the cathode tip. The maximum value of current density is then increased. The shrinking of the cathode arc attachment can also be explained by the cathode surface heating expression $F_{\mathrm{ca}} = -\varepsilon\alpha T_{\mathrm{c}}^4 - j_{\mathrm{e}}\Phi_{\mathrm{c}} + j_{\mathrm{i}}V_{\mathrm{i}} - k\frac{\mathrm{d}T}{\mathrm{d}n}$. The whole plasma column tends to move towards the outlet as inlet velocity increases. The j_{i} and $-k\frac{\mathrm{d}T}{\mathrm{d}n}$ then decrease in the fringe of the arc attachment, inducing the final shrinking effect. The cathode arc attachment of V=0.9 m/s and 1.1 m/s almost copy each other, which indicates that there is a limit for the shrinking of the arc root.

4 Conclusions

This paper has presented a 2D model of the cathode-plasma system, including a simple assumption of heating flux to the cathode. The aim of this paper is to carry out a parametric study on arc and arc attachment behavior, with the existence of an axial magnetic field. Results are obtained for a plasma torch with an arc discharge between a rod-type cathode and a hollow anode. It is shown that:

a. The cathode shape plays a key role in deciding the configuration of the cathode arc attachment. The cathode arc attachment gradually shifts off the axis towards the foot of the conical surface with the increase of the cathode conical angle.

b. The axial thickness of the arc column is highly related to the inlet speed: the plasma column expands more severely in the axial direction near the axis with a higher inlet speed.

c. The external axial magnetic field dramatically affects the position of the cathode arc attachment: the cathode arc root is more diffused and locates farther from the axis with the higher external axial magnetic field.

d. The plasma retains the same shape with the increase of total current. However, the maximum value of plasma temperature and velocity magnitude increase with the total current.

References

1 Baeva M, Kozakov R, Gorchakov S, et al. 2012, Plasma Sources Sci. Technol., 21: 055027

2 Chen D M and Pfender E. 1981, IEEE Trans. Plasma Sci., 9: 265

3 Hsu K C and Pfender E. 1983, Journal of Applied Physics, 54: 4359

4 Gleizes A, Gonzalez J J and Freton P. 2005, Journal of Physics D: Applied Physics, 38: R153

5 Benilov M S and Cunha M D. 2002, Journal of Physics D: Applied Physics, 35: 1736

6 Heberlein J. 2002, Pure and Applied Chemistry, 74: 327

7 Fauchais P. 2004, Journal of Physics D: Applied Physics, 37: R86

8 Xia W D, Li L C, Zhao Y H, et al. 2006, Applied Physics Letters, 88: 211501

9 Li L C. 2008, Experimental observation and numerical analysis of D. C. arc plasmas dispersed by magnetism [Ph.D]. Univesity of Science and Technology of China, Hefei

10 Baeva M and Uhrlandt D. 2011, Plasma Sources Sci. Technol., 20: 035008

11 Bai B, Zha J, Zhang X N, et al. 2012, Plasma Sci. Technol., 14: 118

12 Li L C and Xia W D. 2008, Japanese Journal of Applied Physics, 47: 273

13 Westhoff R and Szekely J. 1991, Journal of Applied Physics, 70: 3455

14 Bauchire J M, Gonzalez J J and Gleizes A. 1997, Plasma Chemistry and Plasma Processing, 17: 409

15 Bianchini R C, Favalli R C, Pimenta M M, et al. 2000, Journal of Physics D: Applied Physics, 33: 134

16 Park J M, Kim K S, Hwang T H, et al. 2004, IEEE Trans. Plasma Sci., 32: 479

17 Cram L E. 1983, Journal of Physics D: Applied Physics, 16: 1643

18 Lowke J J, Kovitya P and Schmidt H P. 1992, Journal of Physics D: Applied Physics, 25: 1600

19 Lowke J J, Morrow R and Haidar J. 1997, Journal of Physics D: Applied Physics, 30: 2033

20 Sansonnens L, Haidar J and Lowke J J. 2000, Journal of Physics D: Applied Physics, 33: 148

21 Zhu P Y, Lowke J J, Morrow R, et al. 1995, Journal of Physics D: Applied Physics, 28: 1369

22 Chen T, Zhang X N, Bai B, et al. 2015, Plasma Chemistry and Plasma Processing, 35: 61

23 Pfender E. 1980, Pure and Applied Chemistry, 52: 1773

24 Yakhot V and Orszag S A. 1986, Physical Review Letters, 57: 1722

25 Yakhot V, Orszag S A, Thangam S, et al. 1992, Physics of Fluids A: Fluid Dynamics, 4: 1510

26 Benilov M S. 1995, Journal of Physics D: Applied Physics, 28: 286

27 Botticher R and Botticher W. 2000, Journal of Physics D: Applied Physics, 33: 367

28 Morrow R and Lowke J J. 1993, Journal of Physics D: Applied Physics, 26: 634

29 Bini R, Monno M and Boulos M I. 2006, Journal of Physics D: Applied Physics, 39: 3253

30 Wang H X and Chen X. 2005, Plasma Sci. Technol., 7: 3051

31 Li L C and Xia W D. 2008, Chinese Physics B, 17: 649

(Manuscript received 3 July 2015)
(Manuscript accepted 6 September 2015)
E-mail address of corresponding author XIA Weidong: xiawd@ustc.edu.cn